SUPPLEMENTARY INFORMATION

Transition metal-doped SrTiO$_3$: when does a tiny chemical impact have such a great structural response?

Mikhail V. Talanov*[a], Adam I. Stash[b], Sergey A. Ivanov[c], Elena S. Zhukova[a], Boris.P. Gorshunov[a], Boris M. Nekrasov[a], Alexander V. Melentev[a], Vladislav I. Kozlov[d,e], Valery M. Cherepanov[f], Sergey.Yu.Gavrilkin[g], Aleksey Yu.Tsvetkov[g], Ilya A. Zavidovskiy[h], Mikhail K. Tatmyshevskiy[h], Maxim Savinov[i], Valeriy M. Talanov[j] and Alexander A. Bush[d]

Experimental

Crystal growth

Single crystals were grown by crucibles zone melting method with optical heating on a URN-2-ZP setup described elsewhere [1]. Pre-synthesized ceramic cylindrical rods with a diameter of 4 mm and a length of 90 mm were used for crystallization. Their composition corresponded to the chemical formulas SrTiO$_3$ and Sr(Ti$_{0.98}$M$_{0.02}$)O$_3$, M = Mn, Ni, Fe. For the synthesis of crystals, the following reagents were used: SrCO$_3$ (99%), TiO$_2$ (98%), Mn$_2$O$_3$ (96%), FeO (98%), and NiO (99%) as well as SrTiO$_3$ single crystals as a seed, previously grown by zone melting. Zone recrystallization of ceramic rods of indicated compositions was carried out in air at a linear rate of 10–15 mm/h and a rod rotation rate of 40–100 rpm. The choice of M = Mn, Ni, Fe concentration (2 at. %) is due to the importance of further comparison with the literature data and the fact that this is the lowest possible composition allowing to find reliable structure-

properties correlations using X-ray diffraction. As a result, single-crystalline cylindrical boules up to 10 mm long and up to 8 mm in diameter were obtained. The boules were transparent in the visible light and had a light-yellow colour for a nominally pure crystal and burgundy, deep pink, and black colours for Mn-, Fe-, and Ni-doped single crystals (Figure S1). The powder diffraction pattern of the crushed crystals taken on a DRON X-ray diffractometer (Cu-Kα radiation) confirms that at room temperature they belong to the cubic phase of STO without any traces of impurity phases.

Single crystal X-ray diffraction

Single crystals with developed faces and linear dimensions indicated in Table 1 were selected for X-ray diffraction analysis. Experimental sets of X-ray diffraction data were collected on single crystal diffractometer Bruker APEX II with detector PHOTON II at 293 K (graphite monochromatic Mo-Kα radiation, $\lambda =$ 0.71073 Å, φ-, ω-scanning). Integration of X-ray diffraction peak intensities was carried out using the SAINT v 8.38A software. The SADABS v 2016/2 program included in the APEX3 package [2] was used to take into account the absorption by crystal habitus and reduce the integral intensities to a uniform scale. The solution of the crystal structure was carried out using the Bruker SHELXTL APEX3 software package [2, 3], the XPREP program was used to determine the space group, and the XT and XL programs to determine the structure and further refinement, respectively. Structural refinements were performed by full-matrix least-squares over $F^2(hkl)$ with structural factors for ions Sr^{2+}, Ti^{4+}, O^{2-}, and M (= Mn, Ni, Fe with different valences). The thermal parameters for all atoms were refined in the anisotropic approximation, except for the Mn atom, which was refined in the isotropic approximation (Table S1). Table 1 shows the parameters of the X-ray diffraction experiment and the final results of crystal structure refinements.

a. Laboratory of Terahertz Spectroscopy, Center for Photonics and 2D Materials, Moscow Institute of Physics and Technology, 9 Institutskiy Pereulok, Dolgoprudny, Moscow Region 141700, Russia

b. A. N. Nesmeyanov Institute of Organoelement Compounds of Russian Academy of Science, 28 Vavilov st., 119991 Moscow, Russia.

c. Chemical Department, Moscow State University, 1 Leninskie Gory, 119991 Moscow, Russia

d. Research Institute of Solid-State Electronics Materials, MIREA – Russian Technological University (RTU MIREA), 78 Vernadsky prospect, 119454 Moscow, RussiaAddress here.

e. Kapitza Institute for Physical Problems RAS, 2 st. Kosygina, 119334 Moscow, Russia

f. National Research Center "Kurchatov Institute", 1 ac. I.V. Kurchatov square, 123182 Moscow, Russia

g. P. N. Lebedev Physical Institute of the Russian Academy of Sciences, 119991 Moscow, Russia.

h. Center for Photonics and 2D Materials, Moscow Institute of Physics and Technology, 9 Institutskiy Pereulok, Dolgoprudny, Moscow Region 141700, Russia

i. Institute of Physics, Czech Academy of Sciences, 18200 Prague 8, Czech Republic

j. Platov South-Russian State Polytechnic University, 346428, Novocherkassk, Russia

* Corresponding Author, e-mail: mvtalanov@gmail.com

Electronic Supplementary Information (ESI) available: See DOI: 10.1039/D4TC00180J

Raman, terahertz, and infrared measurements.

Raman spectra of crystalline samples (Fig. S2-4) were acquired with a Horiba LabRAM HR Evolution (HORIBA Ltd., Kyoto, Japan) confocal Raman microscope in backscattering geometry with excitation wavelength 532 nm. The excitation power density was $\sim$ 130 kW/cm² over a spot area $\sim$ 1.8 µm². Diffraction grating with 600 lines/mm was used to measure spectra from 50 to 1700 cm^{-1}. Each spectrum was averaged over 10 repetitions with 20 s integration time. The samples were checked for homogeneity, and the variation of spectra from different acquisition spots was negligible. Low-temperature measurements were performed in Linkam FTIR600 nitrogen cryostat with ZnSe windows and integrated temperature control system.

For the infrared and terahertz measurements, plane-parallel STO and STO:M (M=Mn, Ni, Fe) with thicknesses $d \approx 0.076$ mm (STO), $d \approx 0.1$ mm (STO:Mn), $d \approx 0.3$ mm (STO:Ni), $d \approx 0.15$ mm (STO:Fe) were cut from bulk single crystals and carefully polished. To check ferroelectric soft mode behaviour, terahertz measurements of real $\varepsilon'(\nu)$ and imaginary $\varepsilon''(\nu)$ parts of the complex dielectric permittivity $\varepsilon^*(\nu) = \varepsilon'(\nu) + i\varepsilon''(\nu)$ were performed using the time-domain spectrometer TeraView TPS Spectra 3000, in transmission geometry at frequencies 5-25 cm^{-1} and temperatures 75-300 K; below 75-100 K (depending on the sample) transmissivity was too low to allow reliable determination. With the measured spectra of $\varepsilon'(\nu)$ and $\varepsilon''(\nu)$, THz reflection coefficient spectra were calculated using standard Fresnel equations, and merged with the measured infrared reflection coefficient spectra. Reflection coefficient spectra in the range $\nu = 40 - 5000$ cm^{-1} were measured using standard vacuum Fourier-transform infrared spectrometer Bruker Vertex 80v.

Dielectric measurements

For dielectric radio-frequency (RF) measurements the base surfaces of the sample were covered by the electrodes which were obtained by burning Ag-paste at $\sim$ 773 K. Low-frequency complex dielectric permittivity $\varepsilon^*(\nu) = \varepsilon'(\nu) + i\varepsilon''(\nu)$ and loss tangent $\tan \delta(\nu) = \varepsilon''(\nu)/\varepsilon'(\nu)$ were measured at frequencies 25 Hz − 1 MHz and temperatures 4.2 K − 294 K using an E7-20 immittance meter (Minsk Scientific Research Instrument Making Institute, Belarus). The temperature rate and applied AC electric field was 2 − 3 K/min and $\sim$ 1 V/mm, respectively. The measurements presented in Fig. S5 were made before and after polishing, followed by burning of the Ag-paste. Dielectric measurements shown in Fig. S6 and S7 were performed before and after annealing at 1400°C, followed by slow (1.2°C/min) cooling.

Mössbauer measurements

Mössbauer spectroscopy measurement was performed at room temperature (293 K) using a conventional constant acceleration type spectrometer (MS-1104Em) in transmission geometry with a 57Co(Rh) source, which had activity of about 5 mCi. Since the effect of the Mössbauer absorption turned out to be quite small (~0.1%), the measurement was performed during a period of 20 days to increase the accuracy of determining the parameters of the Mössbauer spectrum. The obtained Mössbauer spectrum is shown in Fig. S8 and appears as a single broadened line. The spectrum was analyzed by the least square method with the Lorentzian line shape in the model of one doublet using the SPECTR program from the MSTools package. Isomer shift was determined in relation to the centroid of α-Fe. The line width of α-Fe was 0.23 mm/c. The parameters of the doublet are given in Table S2.

The isomer shift value IS = 0.22(9) mm/s is typical for the Fe^{3+} valence state in oxygen pentahedral surroundings and is in accordance with data of [4] where it was shown that iron enters the $SrTiO_3$ lattice substitutionally at the Ti^{4+} site in its high-spin ferric state and is usually associated with a charge-compensating oxygen vacancy.

Magnetic measurements

Measurements of single-crystal samples were carried out in a standard commercial vibration SQUID magnetometer MPMS-XL7 Quantum Design with a sensitivity of $2 \cdot 10^{-7}$ emu, in the temperature range from 300 K to 9 K in a helium atmosphere.

The temperature dependencies of the magnetic susceptibility (Fig. S9) do not show any anomalies associated with known magnetic phase transitions in oxides based on the transition metals.

Energy dispersive analysis

Energy dispersive (EDS) analysis was performed using a Carl Zeiss Ultra 55+ scanning electron microscope (SEM) and an Oxford Instruments X-MAX 80 energy dispersive detector. For Mn- and Fe-doped SRT single crystals, the results are presented in Figures S10, S11 and in Tables S4, S5. The content of Mn and Ni, estimated from several points for each single crystal, is approximately 4.5 at. % and 3.0 at. %.
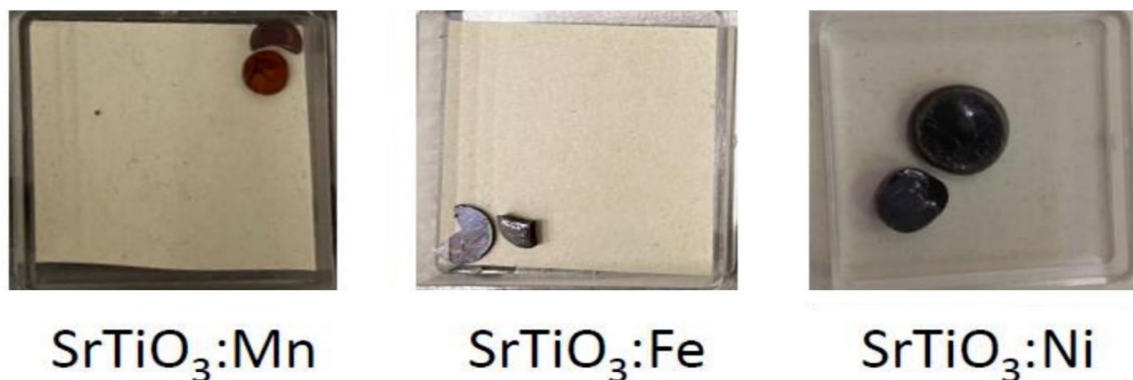
Fig. S1. Photos of grown single crystals.

Table S1   Atomic displacement parameters and occupation factors obtained from X-ray diffraction experiments for the $SrTiO_3$:M (M = Fe, Ni, Mn) and pure $SrTiO_3$ single crystals at room temperature

| Single crystal	Atom	U_{11}, Å^2	U_{33}, Å^2	Site occupation
$Sr(Ti_{0.98}Fe_{0.02})O_3$	Sr	0.00670(11)		1
	Ti	0.0040(3)		0.94(2)
	Fe	0.007(7)		0.010(4)
	O	0.0112(4)	0.0052(5)	0.985(8)
$Sr(Ti_{0.98}Ni_{0.02})O_3$	Sr	0.00699(10)		1
	Ti	0.0047(2)		0.980(12)
	Ni	0.029(15)		0.020(12)
	O	0.0116(3)	0.0056(4)	1
$Sr(Ti_{0.98}Mn_{0.02})O_3$	Sr	0.00712(10)		1
	Ti	0.0044(4)		0.97(3)
	Mn	0.012(10)		0.005(4)
	O	0.0114(4)	0.0056(5)	0.988(9)
$SrTiO_3$	Sr	0.00722(9)		1
	Ti	0.00527(9)		1
	O	0.0117(3)	0.0058(4)	1

SUPPLEMENTARY INFORMATION
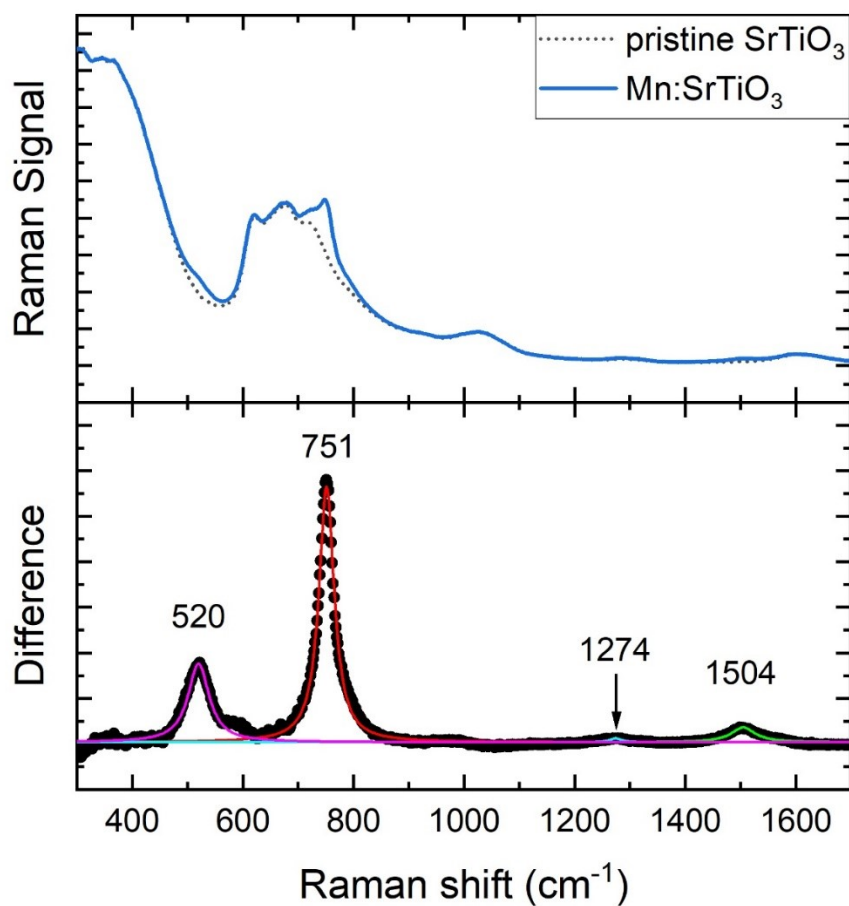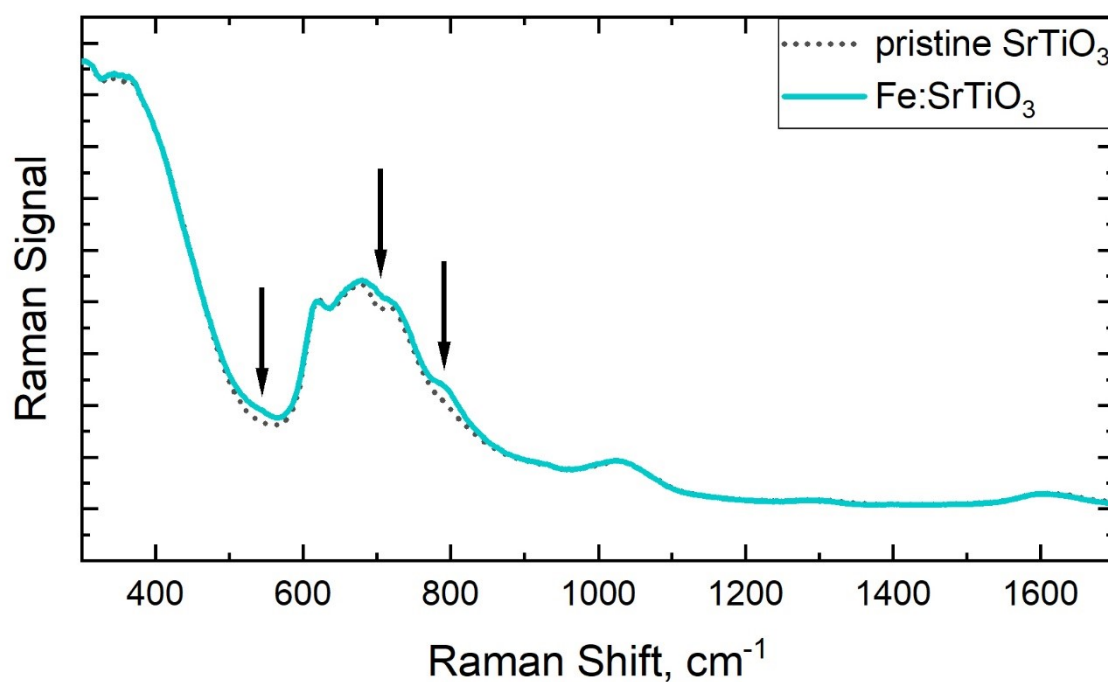

Fig. S2. (top) Room temperature Raman spectrum of 2% Mn-doped STO crystal compared to Raman spectrum of pristine STO crystal. (bottom) Difference of the two spectra fitted with Lorentzian terms. The central frequencies of the two strongest lines are $v_1 = 520$ cm^{-1} and $v_2 = 751$ cm^{-1}, while the two others are 1274 (close to $v_1 + v_2$) and 1504 (close to $2v_2$). This and Lorentzian lineshape of these peaks indicate, that they are not artefacts of difference analysis and correspond to intrinsic modes induced by doping.

Fig. S3. Room temperature Raman spectrum of 2% Fe-doped STO crystal compared to Raman spectrum of pristine STO crystal. Arrows indicate minor differences between the spectra.
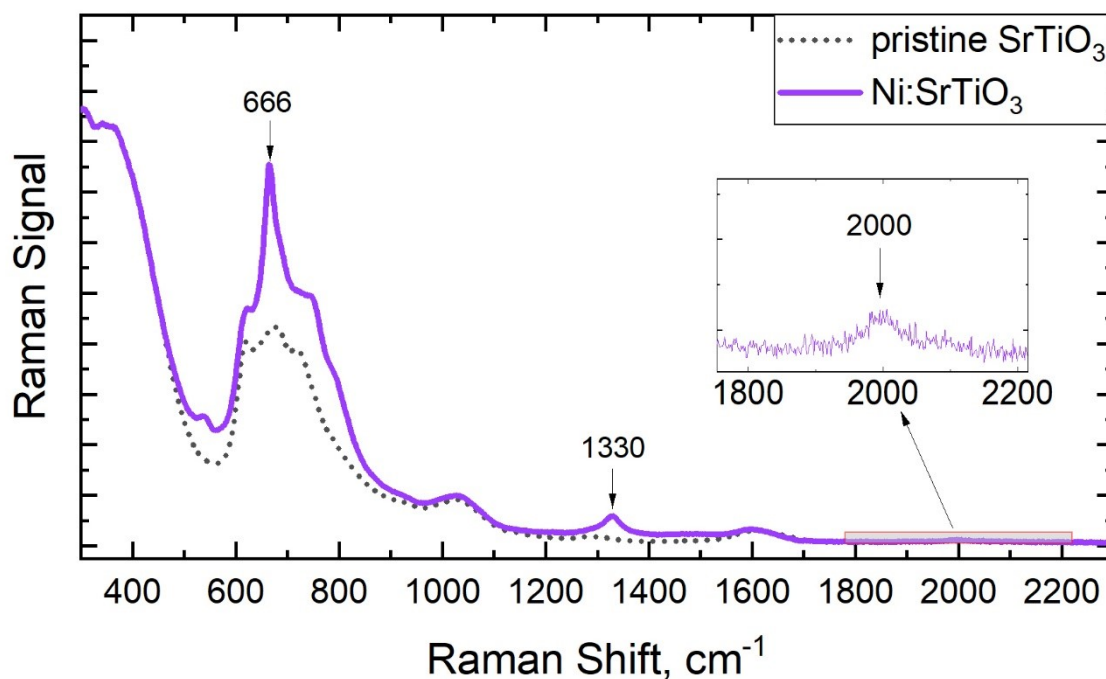

Fig. S4. Room temperature Raman spectrum of 2% Ni-doped STO crystal compared to Raman spectrum of pristine STO crystal. Sharp peak at 666 cm^{-1} is accompanied by two smaller peaks at 1330 cm^{-1} and 2000 cm^{-1}. They correspond to a local mode caused by the replacement of Ti by Ni and its second and third harmonics.
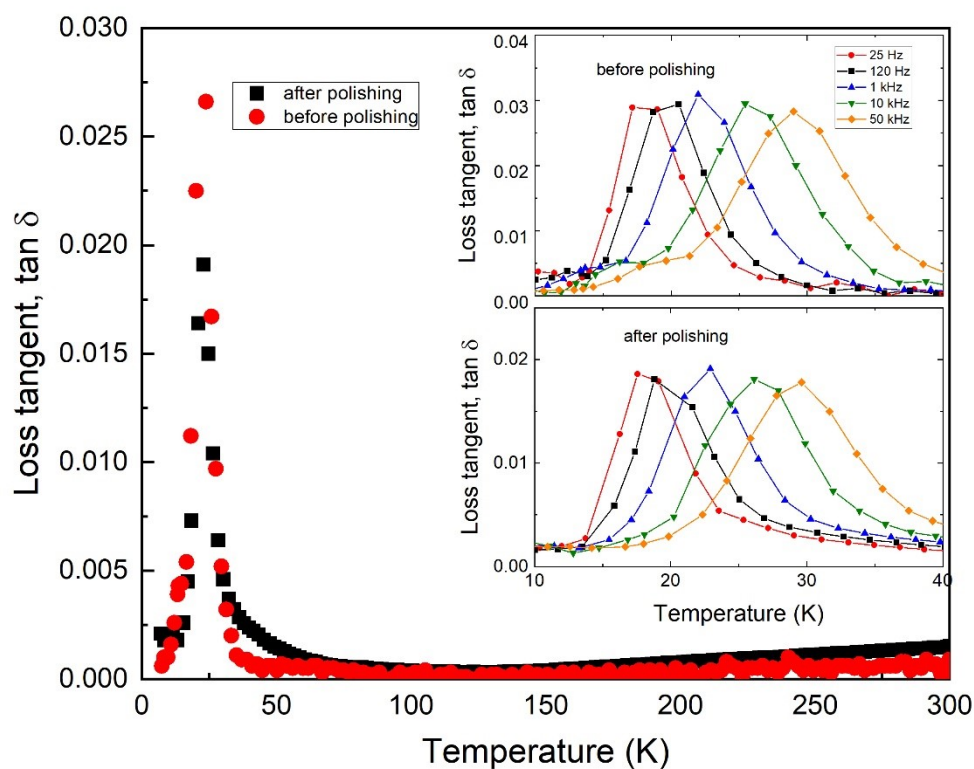
Fig. S5. Temperature dependences of dielectric loss tangent (tan δ) of 2% Mn-doped STO single crystals, measured at 1 kHz before (red) and after (black) mechanical polishing. Insets show temperature dependences of tan δ, measured at different frequencies (f = 25 Hz – 50 kHz). Polishing resulted in a decrease in sample thickness from 0.8 mm to 0.48 mm.
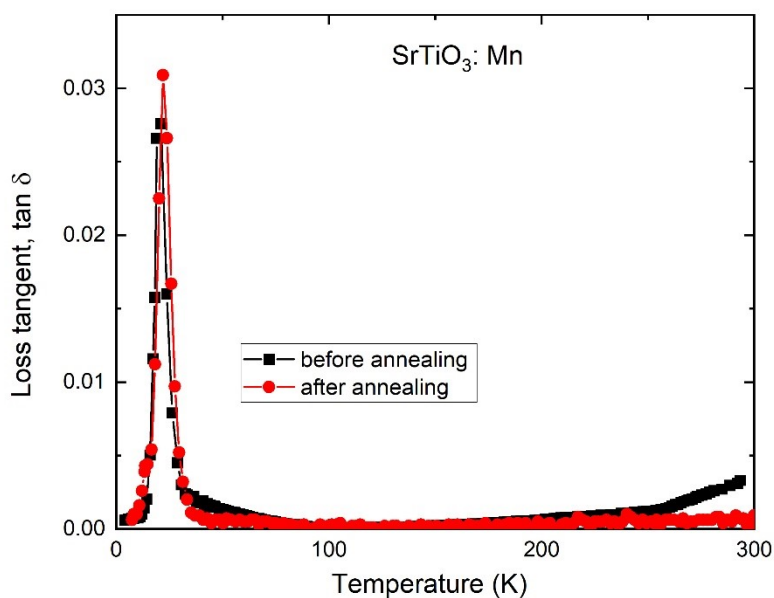

Fig. S6. Temperature dependences of dielectric loss tangent (tan δ) of 2% Mn-doped STO single crystal, measured at 1 kHz before (black) and after (red) high-temperature annealing. Note that similar behavior is observed at all available measuring frequencies.
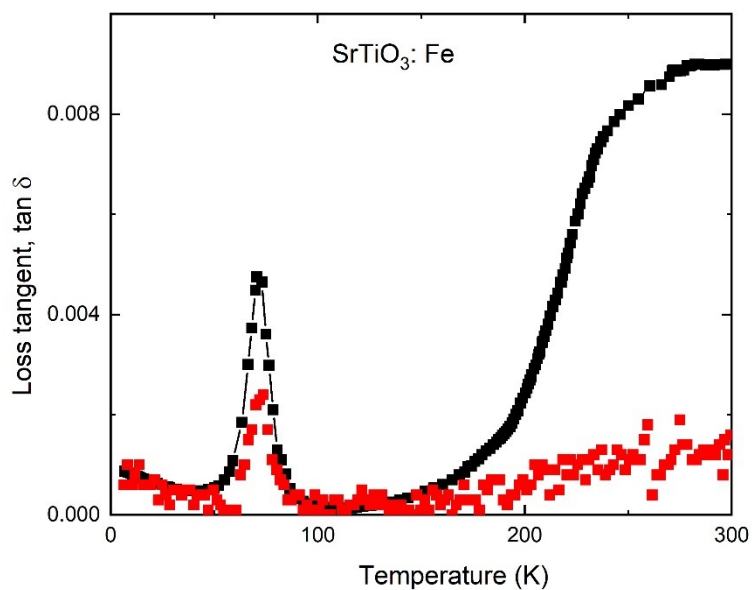
Fig. S7. Temperature dependences of dielectric loss tangent (tan δ) of 2% Fe-doped STO single crystal, measured at 1 kHz before (black) and after (red) high-temperature annealing. Note that similar behavior is observed at all available measuring frequencies.
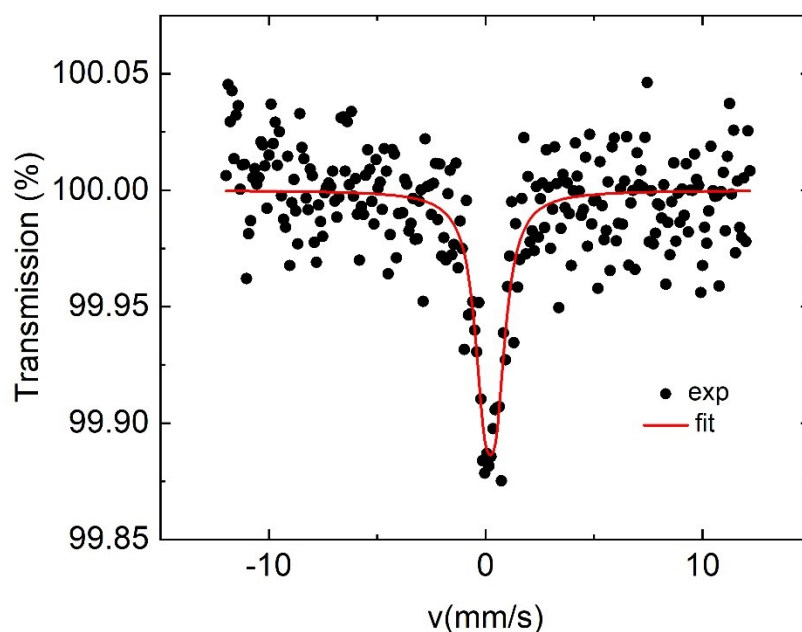

Figure S8. Mössbauer spectrum of the powder sample SrTiO$_3$:Fe obtained at T=293 K. Solid line shows fit by Lorentzian line shape in the model of one doublet.

Table S2. Parameters of the Mössbauer spectra for $SrTiO_3$: Fe single crystals: IS – isomer shift, QS – quadrupole splitting, Γ - line width

Parameter	IS, mm/s	QS, mm/s	Γ, mm/s
Value	0.22(9)	0.54(18)	1.1(2)

Table S3 Shannon ionic radii (R) for Ti^{4+}, M^{n+} (M = Mn, Ni, Fe, n = 3, 4), Sr^{2+} with coordination number (CN) 6 and various spin states (HS – high spin, LS – low spin)

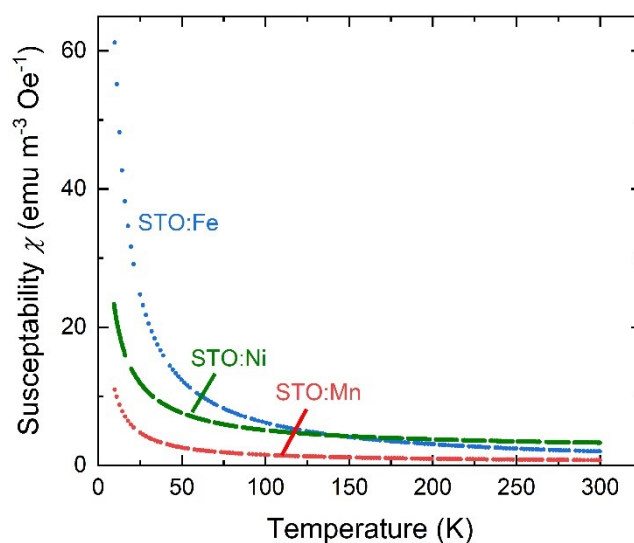| Ion	Ti^{4+}	Mn^{4+}	Mn^{3+}	Mn^{3+}	Ni^{4+}	Ni^{3+}	Ni^{3+}	Fe^{4+}	Fe^{3+}	Fe^{3+}
CN	6	6	6LS	6HS	6 LS	6 LS	6HS	6	6 LS	6 HS
R, Å	0.605	0.53	0.58	0.645	0.48	0.56	0.60	0.585	0.55	0.645

Fig. S9. Temperature dependencies of the magnetic susceptibility of $SrTiO_3$:M (M = Fe, Ni, Mn) single crystals (χ in units [emu*Oe^{-1}m^{-3})]).
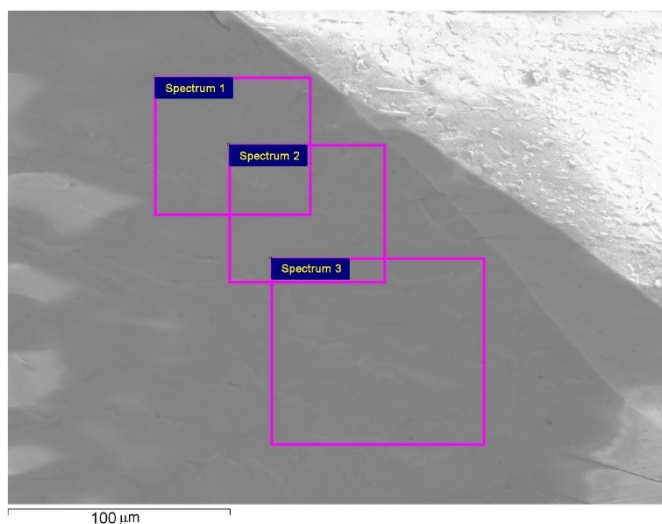
Journal of Materials Chemistry C

Fig. S10. SEM (scanning electron microscopy) - images of the Mn-doped STO single crystal. Squares mark the surface areas for which EDS analysis was carried out.

Table S4. EDS analysis of the Mn-doped STO single crystal. Processing options: all elements analyzed (Normalized)

Spectrum	O	Ti	Mn	Sr
Spectrum 1	57.52	21.38	0.92	20.18
Spectrum 2	57.33	21.72	0.99	19.96
Spectrum 3	61.81	20.05	0.89	17.25
Average	58.89	21.05	0.93	19.13
Std. deviation	2.54	0.89	0.05	1.63
Max	61.81	21.72	0.99	20.18
Min	57.33	20.05	0.89	17.25

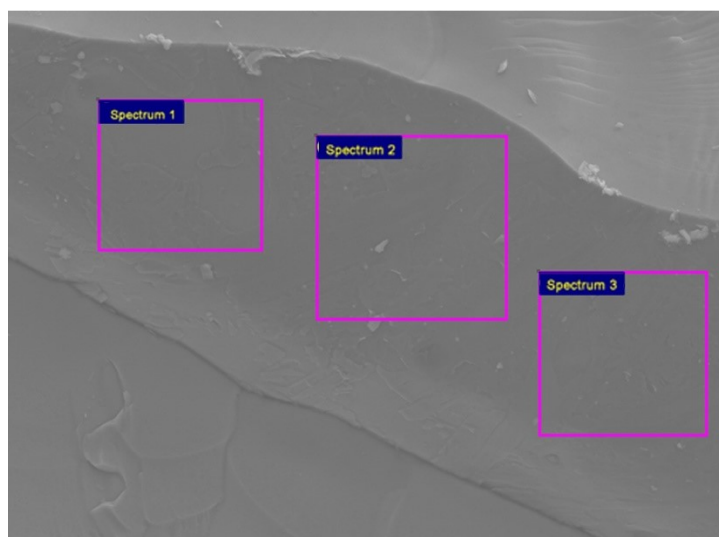All results are in normalized atomic %

Fig. S11. SEM (scanning electron microscopy) images of the Ni-doped STO single crystal. Squares mark the surface areas for which EDS analysis was carried out.

Table S5. EDS analysis of the Ni-doped STO single crystal. Processing options: all elements analyzed (normalized)

Spectrum	O	Ti	Ni	Sr
Spectrum 1	59.66	20.60	0.47	19.27
Spectrum 2	62.76	20.25	0.49	16.50
Spectrum 3	57.41	21.38	0.85	20.36
Average	59.94	20.74	0.60	18.71
Std. deviation	2.68	0.58	0.21	1.99
Max	62.76	21.38	0.85	20.36
Min	57.41	20.25	0.47	16.50

All results in normalized atomic %

.

SUPPLEMENTARY INFORMATION

Notes and references

1   A. M. Balbashov and S. K. Egorov, Journal of Crystal Growth, 1981, 52, 498-504.
2   APEX3, SAINT and SADABS, Bruker AXS Inc, Madison, Wisconsin, USA, 2019.
3   G. M. Sheldrick, Acta Crystallographica Section C: Structural Chemistry, 2015, 71, 3-8.
4   V. Bhide and H. Bhasin, Phys. Rev., 1968, 172, 290-294.